ACS APPLIED MATERIALS & INTERFACES

Research Article

Cite This: ACS Appl. Mater. Interfaces XXXX, XXX, XXX−XXX

www.acsami.org

Nonmagnetic Hypertonic Saline-Based Implant for Breast Cancer Postsurgical Recurrence Prevention by Magnetic Field/pH-Driven Thermochemotherapy

Fei Gao,[†,‡] Tingbin Zhang,[†] Xiaoli Liu,[†] Anujit Ghosal,[†] Dan Wang,[‡] Wensheng Xie,[‡] Yongsan Li,[§] Xing Wang,[§,∥] Lei Tao,[§] Jing Yu,[⊥] Yen Wei,*[,§] Hai Ming Fan,*[,†] and Lingyun Zhao*[,‡]

[†]Key Laboratory of Synthetic and Natural Functional Molecule Chemistry of the Ministry of Education, College of Chemistry and Materials Science, Northwest University, Xi'an, Shaanxi 710069, China

[‡]Key Laboratory of Advanced Materials of Ministry of Education of China, Key Laboratory of Advanced Materials of Ministry of Education of China, School of Materials Science & Engineering and [§]Department of Chemistry, Tsinghua University, Beijing 100084, China

[∥]Beijing Laboratory of Biomedical Materials, Beijing University of Chemical Technology, Beijing 100029, China

[⊥]College of Materials Science and Engineering, Zhejiang University of Technology, Hangzhou 310014, China

Supporting Information

ABSTRACT: Magnetic-mediated hyperthermia (MMT) is emerging as one of the promising techniques, which could synergistically treat cancer along with current treatment techniques such as chemotherapy and radiotherapy and trigger on-demand release of therapeutic macromolecules. However, the low specific absorption rate and potential in vivo toxicity of magnetic nanomaterials as the MMT mediators restrict the new advancements in MMT treatment. Herein, for the first trial, the unique inductive heating property of hypertonic saline (HTS), a clinically applied solution exhibiting several physiological effects under alternative magnetic field (AMF), was systematically investigated. Though without magnetic property, due to the dipolar polarization under the electromagnetic radiation, HTS can induce enough high and rapid temperature increase upon exposure under AMF. Based on such an observation, PEG-based HTS hydrogel was fabricated for the inhibition of unwanted diffusion of ions so as to ensure the ideal temperature rise at the targeted region for a longer time. Furthermore, an anticancer drug (doxorubicin) was also incorporated into the hydrogel to achieve the magnetic field/pH stimuli-responsive drug-sustainable release as well as synergistic thermochemotherapy. The potential application of the drug-loaded HTS-PEG-injectable hydrogel for breast cancer postsurgical recurrence prevention is demonstrated. Significant in vivo suppression of two kinds of breast cancer models was achieved by the hybrid hydrogel system. This work explores a new biomedical use of clinical HTS and a promising cancer treatment protocol based on HTS-PEG hydrogel for magnetic hyperthermia combined with stimuli-responsive chemotherapy for breast cancer postsurgical recurrence prevention.

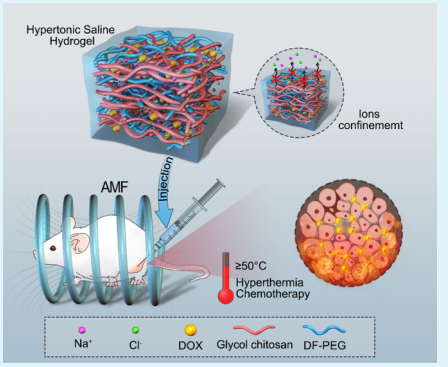

KEYWORDS: *hypertonic saline, magnetic-mediated hyperthermia, dipolar polarization, thermochemotherapy, breast cancer*

INTRODUCTION

Heat treatment of cells and tissues leads to instantaneous molecular and metabolic changes, and therefore hyperthermia combined with radiation or chemotherapy has been rapidly becoming a clinical reality as a form of the treatment of malignant disease.[1] However, the potential advantages of hyperthermia in the management of human cancer could be fully exploited through a heating technique capable of delivering safe, predictable, and reproducible treatment.[1,2] With the working mechanism of heat generation through biomediators under alternative magnetic field (AMF), magnetic-mediated hyperthermia (MMH) has been recently considered as a renaissance of cancer local treatment modality due to its remarkable low side effects and high treatment efficacy.[3,4] As there is almost no limit for the electromagnetic wave in tissue penetration, MMH, the mini- or noninvasive technique could treat all kinds of solid tumors, even the ones seated in deep anatomical location.[5] Recently, both intensive and extensive investigations have been carried out with MMH, and some research findings have been successfully applied in clinical oncology.[6,7]

Thermal mediators play critical roles in the therapeutic effect of cancer treatment by MMH.[8] So far, milliscaled alloy thermoseeds as well as magnetic fluid composed of magnetic

Received: January 30, 2019
Accepted: February 25, 2019
Published: February 25, 2019

DOI: 10.1021/acsami.9b02013
ACS Appl. Mater. Interfaces XXXX, XXX, XXX−XXX

iron oxide nanoparticles (IONPs) have been applied in MMH clinical oncology. Despite ideal inductive heating property under AMF, the rather complicated and time-consuming macroscopic implant of the thermoseeds limits their further application.[9] Nowadays, injectable magnetic fluid has aroused great interest for MMH applications, which could produce heat via the hysteresis or relaxation losses under the effect of AMF.[10−12] However, the relatively poor energy-transfer efficiency intrinsic with IONPs presents a challenging obstacle, which leads to a requirement for extremely high concentrated IONP suspensions injected within the tumor site.[13,14] Furthermore, although IONPs have been approved by FDA for their clinical application as iron deficiency therapeutics or MRI contrast agent, the re-evaluation of the potential risk of side effects in most cases led to their subsequent withdrawal from the market.[15−17] Therefore, it would be of great clinical significance to develop thermal agents, which possess simultaneously high inductive heating property, ideal biocompatibility, as well as injectable property.

Currently, although special attention has been paid on the development of high-performance thermal mediators for MMH, it seems that such a research was tightly restricted with the scope of magnetic or metallic materials.[18] Here, we should reconsider MMH, which though termed as "magnetic-mediated hyperthermia", it should be clarified that "magnetic" does not necessarily limit the choice of the thermal agents only within magnetic materials. All of the materials, which could induce heat under the AMF, should be considered as the candidate for mediators of MMH. Therefore, a new breakthrough could be made for the development of high-performance MMH mediators.

Defined as any crystalloid solution containing more than 0.9% saline, hypertonic saline (HTS) possesses many theoretical advantages (including small-volume resuscitation, reduction of intracranial pressure, improved hemodynamics, and improved microcirculation and immunomodulation) and has been applied widely in clinical studies.[19−21] For instance, HTS has been used for cerebral edema and elevated intracranial pressure, acute bronchiolitis, and small-volume resuscitation of trauma patients with hemorrhagic shock.[19−22] In the current study, for the first time, our research group observed the extraordinary inductive heating property by the nonmagnetic HTS. A rapid temperature rise was observed when we put the HTS (8% NaCl solution) under AMF (~0.5 MHz), indicating its potential to be used in magnetic hyperthermia field. Moreover, other kinds of inorganic salt solutions have also shown obvious heat generation under AMF exposure, confirming the AMF-induced heating effect of charged ions. Based on such inspiring findings, HTS was further formulated within the PEG-based-injectable hydrogel for the inhibition of unwanted diffusion of ions so as to ensure the ideal temperature rise at the targeted region for a longer time.

Except for high-performance thermal mediator, which simultaneously possesses the unique inductive heating property under AMF, being injectable, as well as biocompatibility, such HTS-PEG hydrogel could act as an ideal carrier for loading other therapeutic formulations. In the current study, a chemotherapeutic agent (doxorubicin) was incorporated into the hydrogel for localized chemotherapy.[23] Such as-prepared drug-loaded HTS-PEG-injectable hydrogel can successfully achieve the pH/AMF dual stimuli-responsive drug delivery and magnetic thermochemotherapy for breast cancer postsurgical recurrence prevention (Scheme 1). Except for pioneering the nonmagnetic high-performance agents for MMH, this work explores a new biomedical use of clinical HTS and a promising cancer treatment protocol based on HTS-PEG hydrogel.

Scheme 1. Schematic Diagram Illustrates Hypertonic Saline Hydrogel for Magnetic Hyperthermia-Mediated Breast Cancer Postoperative Recurrence Prevention

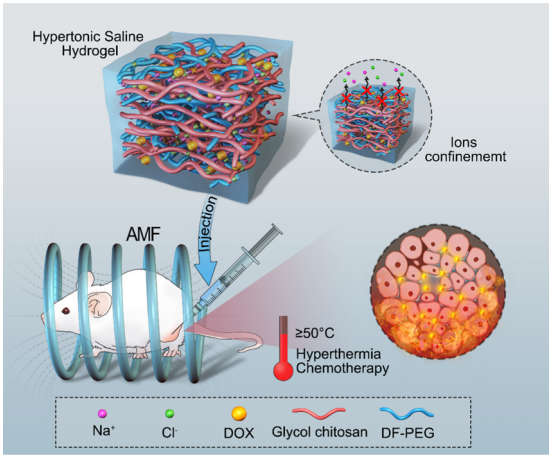

RESULTS AND DISCUSSION

Inductive Heating Properties of HTS Solutions under AMF Exposure. The inductive heating properties of HTS solutions were investigated under AMF with different frequencies (f). As shown in Figure 1, HTS solutions can induce a remarkable temperature increase under AMF, and such an effect was dependent on field intensity (H), frequency, as well as HTS concentration. Figure 1a indicates that no obvious temperature rise was observed when the f is 285 and 370, and 495 kHz frequency would lead to the maximum temperature elevation of around 15 °C. Figure 1b−d remarkably demonstrates the higher field intensity and HTS concentration, and a higher temperature could be achieved. Notably, when H = 150 Oe, even a 20% HTS could not elevate the ΔT to above ~15 °C; however, the alteration of H to 220 and 285 Oe for 15% HTS raises the temperature to above 20 °C within 4 and 2.5 min, respectively. The thermal images (Figure S1) of HTS at different concentrations with AMF exposure were also taken, demonstrating a rather homogeneous temperature distribution within the HTS solutions. It can also be noticed that the deionized water and solid HTS could not be heated under the same field parameters (Figure 1e−f). It means that the charged ions (saline) can induce heat under AMF exposure with higher frequency. On the basis of the results, the hyperthermia temperature with a lower saline concentration (15% HTS) and AMF intensity (H = 220 Oe) was chosen for further investigation.

Mechanism Analysis of Ion Heating under AMF Exposure. The underlying mechanism involved in the heating of HTS under AMF exposure was studied. Except for testing the inductive heating properties of sodium chloride solutions, further on, the inductive heating profiles (under different field intensities (H), 495 kHz) of many different kinds of salt solutions were also evaluated. As shown in Figure 2a−d, a similar trend was observed, where all of the salt solutions can be heated under AMF exposure and the heating capacity can

DOI: 10.1021/acsami.9b02013
ACS Appl. Mater. Interfaces XXXX, XXX, XXX−XXX

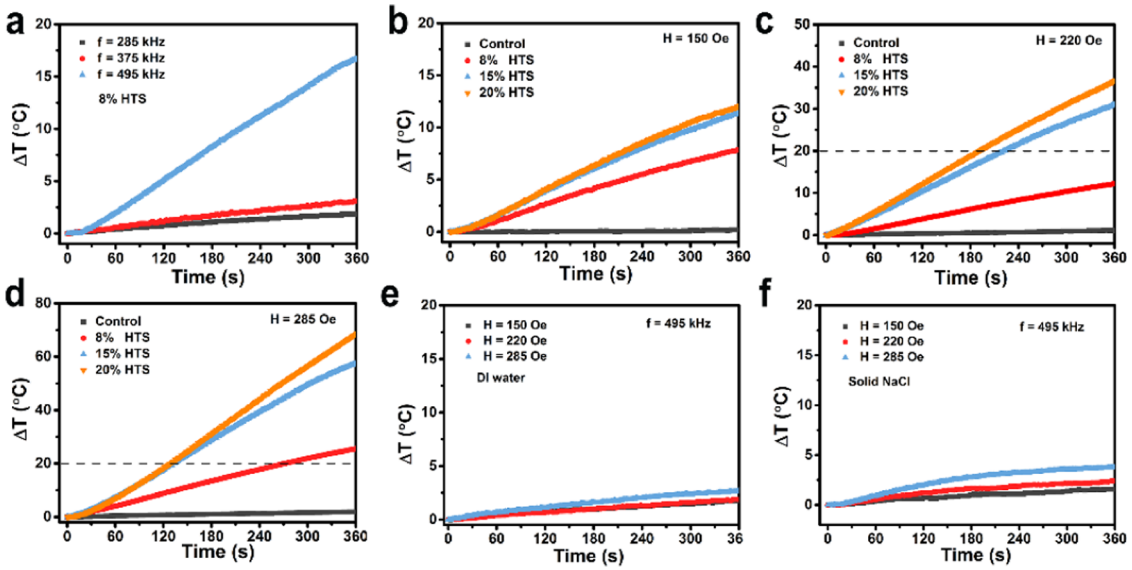

Figure 1. (a) Magnetic heating profiles of 8% HTS under AMF exposure with different frequencies. (b–d) Magnetic heating profiles of HTS with different saline concentrations under AMF exposure with various field intensities. (e, f) Magnetic heating profiles of water and solid NaCl under AMF exposure with various field intensities.

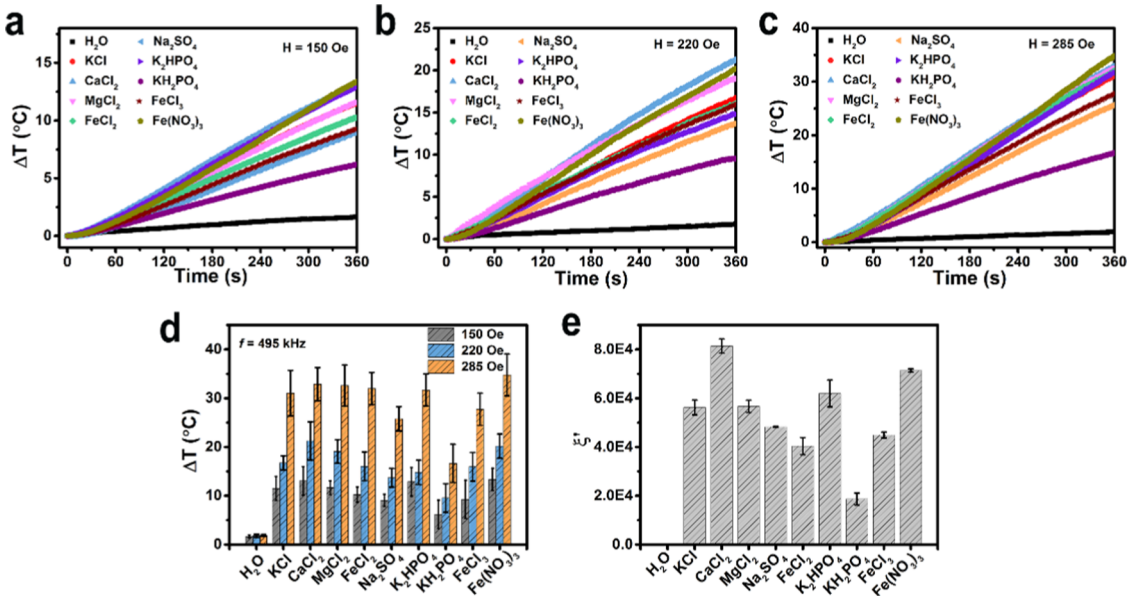

Figure 2. (a–c) Magnetic heating profiles of different kinds of salt solutions (1.0 M) under AMF exposure with different field intensities. (d) Summary of magnetic heating profiles of different kinds of salt solutions. (e) Dielectric constant of different kinds of salt solutions (495 kHz, 25 °C).

be improved by tuning the H value. For example, at a fixed molar mass (1.0 M), after AMF exposure (H = 220 Oe) for 6 min, the temperature elevations for KH_2PO_4, $CaCl_2$, and $Fe(NO_3)_3$ solutions were 9.55, 21.25, and 20.2 °C, respectively. The other salt solutions can promote the temperature increase between 10 and 21 °C.

To elucidate the underlying mechanism involved in the heating of HTS under AMF exposure, the dielectric constant (ε') values of KH_2PO_4, $CaCl_2$, and $Fe(NO_3)_3$ solutions (495 kHz and 25 °C) were measured and are presented in Figure 2e. It can be noticed that there was an existing positive correlation between ε' and inductive heating property, as the salt solution with a higher dielectric constant coincides with the higher heating efficiency. The ε' values of HTS also increased with the increase of saline concentrations (6.08×10^4, 1.14×10^5, and 1.54×10^5 for 8, 15, and 20% saline solutions, respectively), which coincide with the trend in temperature rise (Figure S2). Such observations indicate that the AMF-induced heating effect may be due to the interaction of charged ions with the electromagnetic radiation.[24,25] The electric field causes both permanent and induced dipoles to rotate as they align themselves with the alternating field. The molecular movement generates friction among the rotating molecules, and subsequently, the energy is dissipated as heat (called dipolar polarization).[25] The ability of materials heated in the presence of an electromagnetic field is defined by its dielectric loss tangent: $\tan\delta = \varepsilon''/\varepsilon'$. The dielectric constant (ε') determines how much of the incident energy is reflected and

DOI: 10.1021/acsami.9b02013
ACS Appl. Mater. Interfaces XXXX, XXX, XXX–XXX

how much is absorbed, whereas the dielectric loss factor (ε'') measures the dissipation of electric energy in the form of heat within materials.[24] For the optimum energy coupling, a moderate value of ε' should be combined with high values of ε'' (to get higher values of tan δ) to convert electromagnetic energy into thermal energy. Further, the electromagnetic wave heating of a dielectric material offers a number of advantages over conventional heating methods: (i) noncontact (remote) heating, (ii) quick start-up and stopping, (iii) selective material heating, (iv) heating from the interior of the material body, and (v) higher level of automation and safety.

Fabrication and Rheology Analyses of HTS-PEG Hydrogel. Direct injection of HTS into the lesion site will lead to the diffusion of ions into the normal tissue surrounding as well as permeate quickly.[26] The leakage of ions will induce unwanted heating and inhibit the in vivo application of the HTS. Considering the ion confinement effect of the hydrogel formulations,[27,28] we prepared the PEG-based biocompatible hydrogel, which cross-linked glycol chitosan solution with aldehyde-modified PEG_{2000} ($DF\text{-}PEG_{2000}$) through the Schiff base linkage. The injectability of the PEG hydrogel has been confirmed by our previous investigation.[29] The HTS was loaded into it through the simple mixing method. SEM images (Figure 3a) show that the microstructural morphologies of the

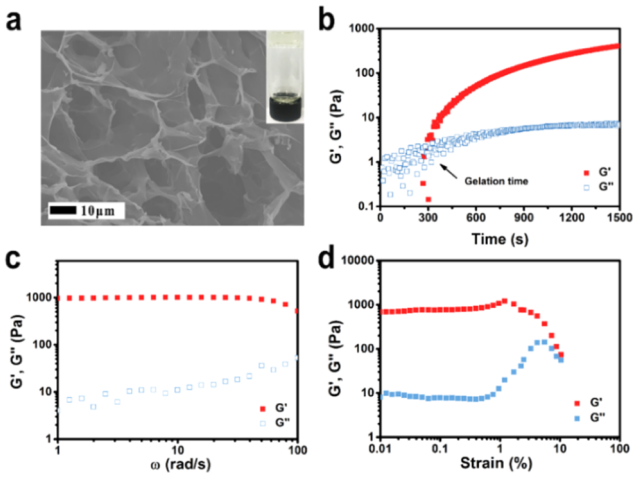

Figure 3. (a) SEM images of the lyophilized HTS-PEG hydrogel. The inset image is the photograph of HTS-PEG hydrogel. (b) Storage modulus (G') and loss modulus (G'') analyses during the gelation process (25 °C; frequency: 1.0 Hz; strain: 5.0%). G' and G'' versus angular frequency (c) and on strain amplitude sweep (d) at a fixed angular frequency for HTS-PEG hydrogel.

freeze-dried HTS-PEG hydrogel exhibited micropores ranging from 5 to 30 μm, which may govern how drugs diffuse inside the hydrogel network and provide efficient spaces for drug transport.[30] The chemical structures of GC, $DF\text{-}PEG_{2000}$, and HTS-PEG hydrogel were characterized by Fourier-transform infrared (FT-IR) spectroscopy (Figure S3). The peak at 1719 cm^{-1} appeared in $DF\text{-}PEG_{2000}$ was attributed to the stretching vibration of the C═O bond in the aldehyde group. However, the aldehyde peak almost disappeared during the hydrogel formation, due to the characteristic absorption of the newly formed Schiff base (at 1644 cm^{-1}).[31]

Measurements of the storage modulus (G') and loss modulus (G'') versus time were performed to monitor the gelation process. As shown in Figure 3b, the gelation time of the hydrogel was ~350 s at 25 °C, which allowed plenty of time for the low-viscosity operation at room temperature. The G' versus shear stress and frequency was carried out (Figure 3c,d), and the samples were prepared and incubated at 37 °C for 20 min. The G' decreased quickly when the strain was ≥10%, and the G' remained stable when the frequency (ω) changed from 1 to ~40. The data of rheology analysis is similar to that described in the literature, i.e., the HTS addition did not influence the intrinsic properties of the dynamic PEG-based hydrogels.[32]

Inductive Heating Property of HTS-PEG Hydrogel. Inductive heating property of 15% HTS-PEG hydrogel under AMF exposure with different field intensity was measured and is shown in Figure 4a. It can be observed that ion confinement

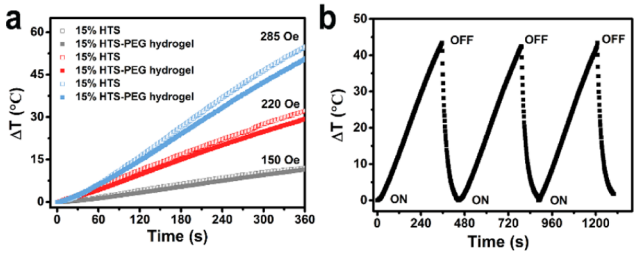

Figure 4. (a) Heating behavior of HTS and HTS-PEG hydrogel under AMF exposure with different field intensity. (b) Magnetic hyperthermia stability with the HTS-PEG hydrogel under AMF exposure for three cycles (495 kHz, 220 Oe).

by the hydrogel formulation only imposes a little effect on the heating property of HTS. For example, at 220 Oe, the 15% HTS could induce a 32.1 °C temperature increase after a 6 min AMF exposure, and the data for 15% HTS hydrogel is about 29.3 °C. The little decrease in temperature elevation may due to the variation of specific heat of water and hydrogel. Moreover, as repeated or multiple hyperthermia treatment is normally adopted other than single treatment in clinical oncology, therefore, the reproducibility of temperature rise is of great clinical significance.[33] As shown in Figure 4b, when HTS-PEG hydrogel was subjected to three rounds of repeated exposure using AMF on/off cycling, a rather reproducible temperature profile was obtained, which suggested the superior stability of HTS-PEG hydrogel against the exposure to the magnetic field.

Ion Confinement Effect of HTS-PEG Hydrogel. Confinement of the charged ions within hydrogel was studied to reduce their diffusion and permeation, avoiding the unnecessary heating in healthy tissue around the tumor and potential side effects. There are many factors that influence the confining capacity of the hydrogel, such as cross-linking density, mesh size, equilibrated water content, and so on.[27] We used an ager phantom that consists of 4% (w/w) agar powder, 0.6% (w/w) NaCl, and 95.4% (w/w) water to mimic the normal tissue around the tumor, followed by the addition of the HTS-PEG hydrogel onto the phantom. Subsequently, the temperature of different sites ($T1$, $T2$, and $T3$) at various time intervals was assessed to monitor the ion diffusion and heating process (Scheme 1).

As shown in Figure 5a–d, $T1$ represents the hyperthermia temperature (tumor) induced by HTS-PEG hydrogel. At the beginning (0 h), the increase of temperature was up to 46.3 °C, whereas after 24 and 48 h diffusions, the ΔT decreased to 37.8 and 34.6 °C. The decrease in the heating capacity

DOI: 10.1021/acsami.9b02013
ACS Appl. Mater. Interfaces XXXX, XXX, XXX−XXX

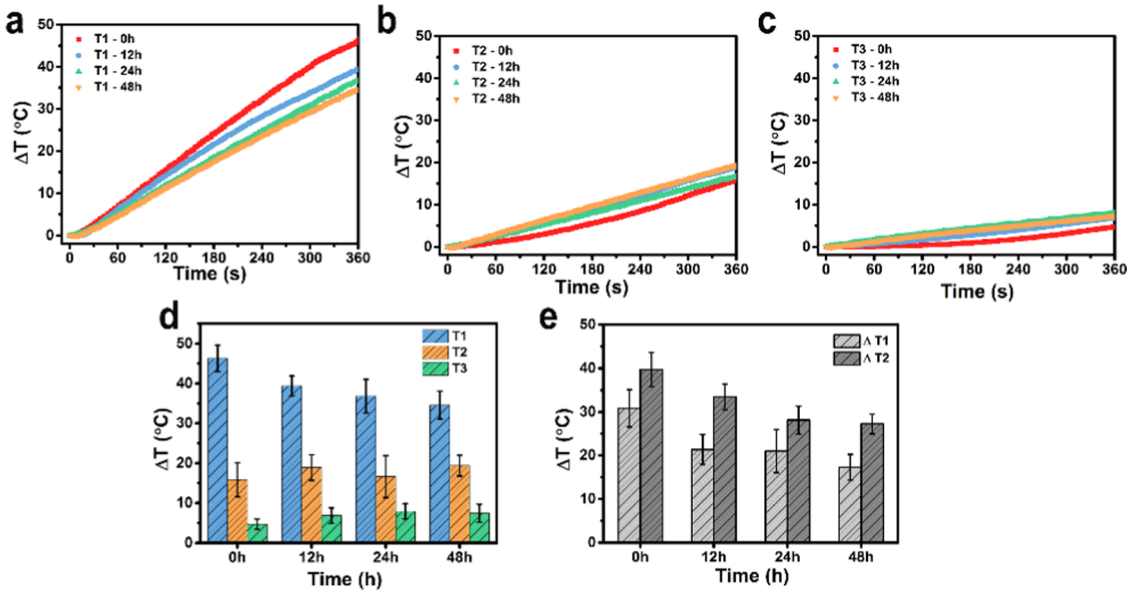

Figure 5. (a–d) Temperature at different locations on centrifugal tubes with AMF exposure for 6 min at different time intervals. *T*1, *T*2, and *T*3 represent the temperature of magnetic hyperthermia, the temperature around the tumor, and the temperature of normal tissue far from the tumor site, respectively. (e) Difference in temperature between *T*1 and *T*2 ($\Delta T1$), and *T*1 and *T*3 ($\Delta T2$) at different time intervals.

indicated the diffusion of some ions in the agar phantom due to the sufficient concentration gradient. Although there is a certain degree of reduction in temperature, the ΔT still can reach the hyperthermia temperature (>25 °C) within 3 min. Temperature around the tumor was represented by *T*2, and at first, the ΔT reached around 15.84 °C; however, after a 48 h diffusion period, the temperature change conversely enhanced to 19.6 °C. The increase in heating most likely originated from the thermal radiation from the HTS-PEG hydrogel and ion diffusion. The little diffused ions do not have a significant effect on the temperature rise. *T*3 represented the normal tissue temperature, far from the tumor site. During the process of diffusion, the ΔT was maintained around 6–7 °C. So, the normal tissue would not get affected by the ion diffusion effect. We also calculated the temperature difference between *T*1 and *T*2 ($\Delta T1$), and *T*1 and *T*3 ($\Delta T2$). As shown in Figure 5e, after 48 h diffusion, they all decreased to a certain extent, for example, at 0 h, the $\Delta T1$ and $\Delta T2$ are 30.82 and 39.71 °C, but after 24 h, both decreased to 20.98 and 28.1 °C, respectively. It also confirmed that parts of the ions diffused into the agar phantom, but the temperature difference can guarantee the therapeutic effect with no or less harm to the normal tissue. All of the results demonstrate that the PEG-based hydrogel network (cross-linked by Schiff's base) could confine most of the charged ions in the desired location due to the homogeneousness throughout the network. The confining capacity may be decided by ion diffusion path length due to the combination of hydrodynamic drag and the obstruction effects.[27] Thus, the hyperthermia temperature can be well obtained even after 48 h of the hydrogel implantation; meanwhile, the normal tissue far away from the tumor does not get interfered.

In Vitro Degradation Behavior and pH- and AMF-Dependent Drug Release. The hydrogel should be designed to be biodegradable to avoid surgical removal after the completion of therapeutic treatment.[34] To investigate the hydrolytic degradation behavior of HTS-PEG hydrogels, the hydrogels were evaluated as a function of incubation time in PBS at different pH values (7.4 and 6.5). As shown in Figure 6a, at pH = 7.4, after 10 days of incubation, the weight losses

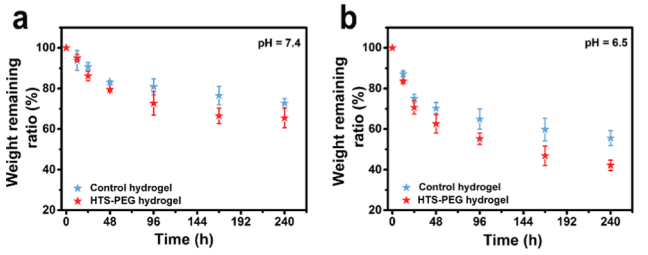

Figure 6. (a, b) In vitro degradation profiles of the control hydrogel and HTS-PEG hydrogel in PBS at pH values 7.4 and 6.5.

were 27.26 and 35.5% for control and HTS-PEG hydrogel, respectively. The higher weight loss for HTS-PEG hydrogel may be due to the following reasons. The ions may decrease the swelling ratio of the hydrogel (Donnan equilibrium theory), and the distinction in the concentration of mobile ions between the hydrogel and external solution was reduced.[35−37] The osmotic swelling pressure of mobile ions inside the hydrogel decreased and the hydrogel structure gets collapsed easily. The hydrolytic degradation was systematically studied under acidic microenvironment (PBS, pH = 6.5). Weight losses of 45.47 and 57.81% for control and HTS-PEG hydrogel were observed after 10 days of incubation (Figure 6b). The faster hydrolytic biodegradation compared to physiological condition may be attributed to the reduced stability of Schiff base bonds in the acidic environment because of the protonation of the amino group within the chitosan molecules.[38] Faster hydrolytic biodegradation of hydrogel within the tumor tissue (acidic microenvironment) was inferred, leading to pH gradient degradation process and drug release profile compared to that of the normal tissue.

The incorporation of anticancer drugs into the hydrogel and exposure with AMF, the smart drug carrier, would have the capacity to accelerate the chemotherapeutic agent's release

DOI: 10.1021/acsami.9b02013
ACS Appl. Mater. Interfaces XXXX, XXX, XXX−XXX

simultaneously with the magnetic hyperthermia treatment.[39] Here, DOX was loaded into the hydrogel formulation to investigate the drug-releasing behaviors of HTS hydrogels. In Figure 7a, the DOX release from hydrogels was found to be in a sustained manner and presented a pH-sensitive release profile. The release rate of DOX from the control hydrogel and HTS-PEG hydrogel gets increased significantly on decreasing the pH from 7.4 to 6.5. As observed, after 12 h incubation, 56.73 and 60.44% of DOX were released from the DOX-loaded control and HTS-PEG hydrogel at acidic pH (6.5), whereas only 35.3 and 39.68% were released at physiological pH (7.4). Reasonably, the higher solubility of DOX at lower pH and the increased degradation of hydrogel lead to a cumulative drug release.[40,41] Other than the internal stimulus, drug release can often be facilitated by the external stimulus such as AMF (Figure 7b). In an 8 h time interval, around 45.58% DOX was released in an acidic pH of 6.5, whereas under AMF exposure, 53.59% of DOX was released in the same time period. A similar trend of increased drug release on AMF exposure was observed at a physiological pH value (Figure S4). The enhanced drug release may be caused by the induced heating effect under AMF exposure, which in turn

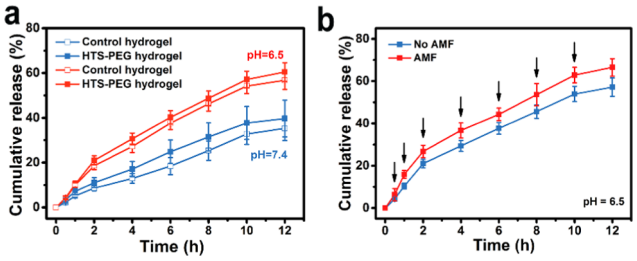

Figure 7. (a) In vitro drug cumulative release profiles of HTS-PEG hydrogel at pH values 7.4 and 6.5. (b) In vitro drug cumulative release profiles of HTS-PEG hydrogel with or without AMF exposure at pH = 6.5. ↓: AMF exposure for 10 min.

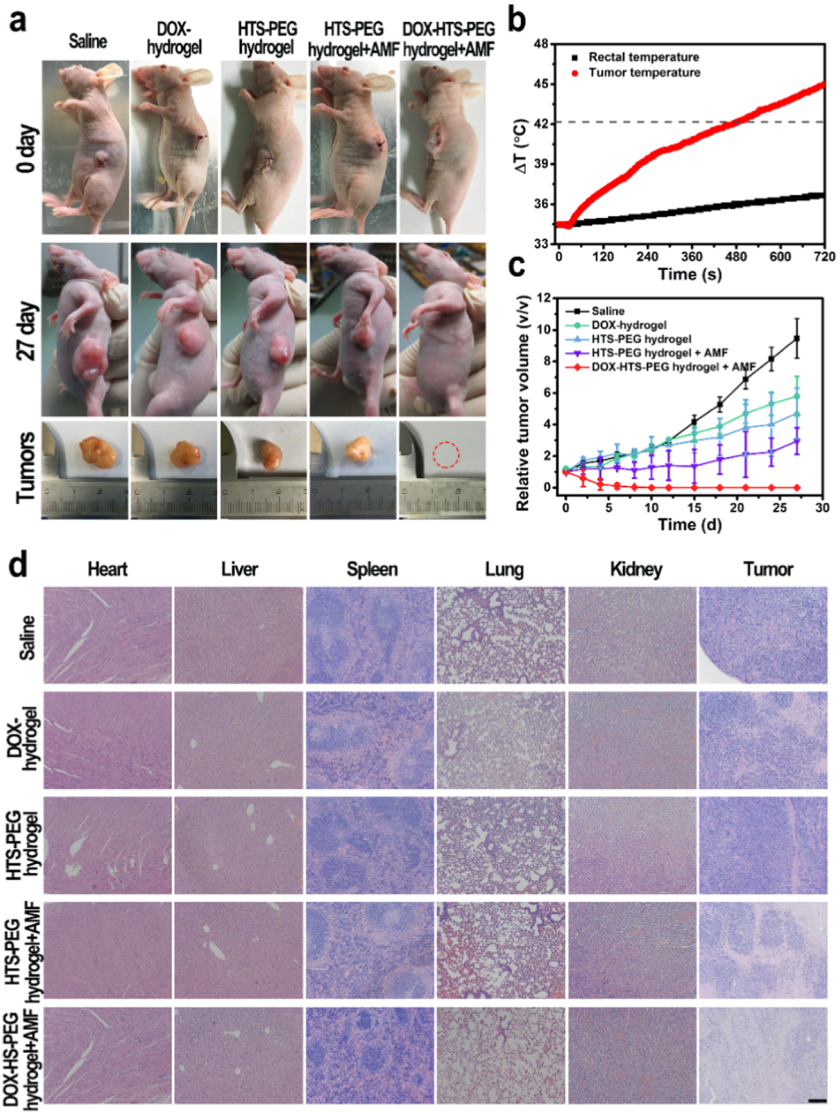

Figure 8. (a) Photographs of MCF-7 tumor-bearing mice before and after 27 days of treatment with saline, DOX-hydrogel, HTS-PEG hydrogel, HTS-PEG hydrogel + AMF, and DOX-HTS-PEG hydrogel + AMF, and representative images of tumor sections harvested from various treatment groups. (b) Tumor site and rectal temperature of tumor-bearing mice treated with HTS-PEG hydrogel + AMF. (c) Changes in relative tumor volumes over time. (d) Histological evaluations of heart, liver, spleen, lung, kidney, and tumor with H&E staining in mice treated with various formulations. The scale bar is 100 μm.

DOI: 10.1021/acsami.9b02013
ACS Appl. Mater. Interfaces XXXX, XXX, XXX−XXX

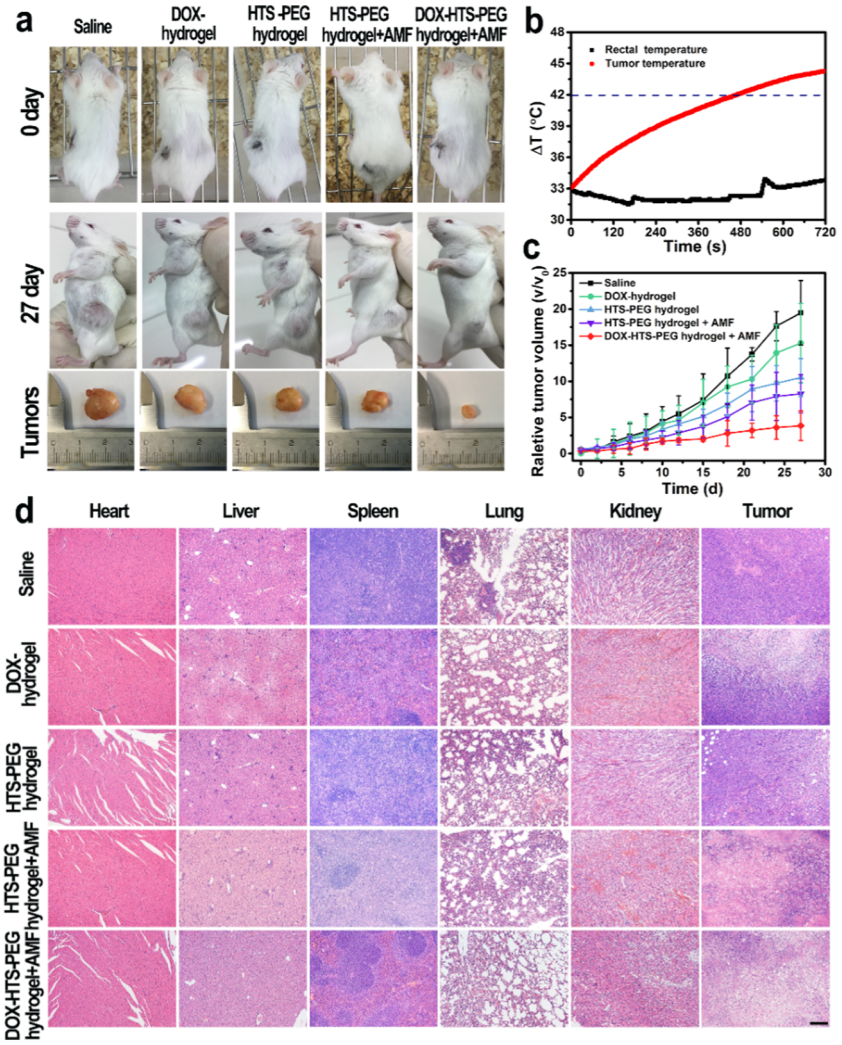

Figure 9. (a) Photographs of 4T1 tumor-bearing mice before and after 27 days of treatment with saline, DOX-hydrogel, HTS-PEG hydrogel, HTS-PEG hydrogel + AMF, and DOX-HTS-PEG hydrogel + AMF, and representative images of tumor sections harvested from various treatment groups. (b) Tumor site and rectal temperature of tumor-bearing mice treated with HTS-PEG hydrogel + AMF. (c) Changes in relative tumor volumes over time. (d) Histological evaluations of heart, liver, spleen, lung, kidney, and tumor with H&E staining in mice treated with various formulations. The scale bar is 100 μm.

expanded the hydrogel networks and accelerated the diffusion of drug molecules.[42] The HTS-PEG hydrogel under AMF exposure can induce magnetic heating and control drug release behavior. The therapeutic effects are highly localized, which greatly enhanced the performance of encapsulated DOX and significantly reduced side effects.

In Vivo Antitumor Efficacy of the DOX-Loaded HTS-PEG Hydrogel. To evaluate the antitumor efficacy of the DOX-loaded HTS-PEG hydrogel for postsurgical recurrence prevention, two breast tumor models, MCF-7 human breast adenocarcinoma tumors and 4T1 murine breast tumors, were employed in the current study. As mentioned above, tumor-bearing mice were randomly assigned into five groups under different treatments: saline (group 1), DOX-hydrogel (group 2), HTS-PEG hydrogel (group 3), HTS-PEG hydrogel + AMF (group 4), and DOX-HTS-PEG hydrogel + AMF (group 5). After surgical removal of the bulky tumor tissues, the hydrogels with different formulations were implanted. After 24 h, mice in groups 4 and 5 were exposed under an AMF (H = 220 Oe, f = 495 kHz) for 12 min. For the MCF-7 tumor-bearing mice, the photographs of the mice and tumors before and after treatment are presented in Figure 8a for each group. The surface temperature of tumor that was treated with HTS-PEG hydrogel increased rapidly and reached ∼43 °C within 480 s; the temperature of mice rectum promoted less than 4 °C during the 10 min AMF exposure (Figure 8b). The relative tumor volume changes as a function of time were plotted (Figure 8c). A slight inhibition of tumor growth by DOX-hydrogel, HTS-PEG hydrogel, or HTS-PEG hydrogel + AMF was observed in the first 10 days, but the tumor began to grow gradually in the next 2 weeks. It suggested that the incomplete ablation of tumor cells and residual cancer cells causes the local recurrence on treatment by chemotherapy and thermotherapy alone. In contrast, only the tumor of DOX-HTS-PEG hydrogel + AMF group was completely eliminated, showing a remarkable synergistic effect of chemotherapy and HTS-PEG hydrogel-induced magnetic hyperthermia therapy. To further evaluate the in vivo therapeutic effect, the main organs (heart, liver, spleen, lung, and kidney) and tumor regions of the mice were harvested and sliced for staining with hematoxylin and eosin (H&E) (Figure 8d). The combined therapy using DOX-HTS-PEG hydrogel + AMF exhibited the largest necrosis area

DOI: 10.1021/acsami.9b02013
ACS Appl. Mater. Interfaces XXXX, XXX, XXX−XXX

extensive fragmentation and obvious nuclear shrinkage, indicating significant cell death. Meanwhile, the morphological evaluation of H&E-stained major organs (Figure 8d) and the body weight of the mice treated with various methods (Figure S5a) was not obviously influenced when compared to that of the control group, showing the excellent security and biocompatibility of HTS-PEG hydrogel system.

As for the 4T1 tumor-bearing mice, the HTS-PEG hydrogel-based synergistic therapy system had a similar effect to inhibit the recurrence. The average tumor size of DOX-HTS-PEG hydrogel + AMF group was the smallest among all groups (Figure 9a,c); the HTS-PEG hydrogel after AMF exposure could promote the temperature of tumor site above 42 °C (mild magnetic hyperthermia, Figure 9b); the H&E-stained tumor section exhibited the largest necrosis area with combined therapy (Figure 9d) and the H&E-stained major organs (Figure 9d) and the body weight of the mice (Figure S5b) also confirmed the biocompatibility of the hydrogel therapeutic system. Notably, the tumor was not completely eliminated, and except for the combined treatment group, a certain amount of tumor metastasis to the lung can be seen in other groups of mice (Figure 9d). The results demonstrated that the 4T1 tumor cells were prone to metastasize highly aggressively and the HTS-PEG hydrogel system could inhibit the lung metastasis of 4T1. All of these results revealed that the developed hybrid hydrogel system with the synergistic enhancement of antitumor effect can be a highly efficient postoperative adjuvant therapeutic approach to largely minimize the risk of recurrence.

CONCLUSIONS

In summary, we have successfully applied the nonmagnetic materials—HTS-induced magnetic heating effect in the biomedical field. The AMF-induced hyperthermia mechanism of HTS was the dipolar polarization of charged ions with high-frequency electromagnetic radiation. The charged ions were confined into the biocompatible hydrogel and utilized in the prevention of breast cancer postoperative recurrence. The AMF-induced hyperthermia behavior and dual stimuli-responsive (pH and AMF) DOX release of these hydrogels were studied. The hybrid hydrogel formulation could be rapidly heated with AMF exposure, and the anticancer drug release could be accelerated under acid tumor microenvironment and magnetic heating effect. In summary, the hybrid hydrogel facilitates chemothermal cotherapy and effectively prevents local breast cancer recurrence in two kinds of breast cancer mouse models. The biocompatible HTS will open a new avenue to apply the nonmagnetic materials in magnetic hyperthermia field.

MATERIALS AND METHODS

Reagents and Chemicals. Agar powder, sodium chloride (NaCl), calcium chloride ($CaCl_2$), potassium chloride (KCl), and other inorganic salts were supplied by Sinopharm Group Co. Ltd. (Shanghai, China). Glycol chitosan (GC, 430 kDa) with 75% deacetylation was purchased from Wako Pure Chemical Industries Ltd. (Tokyo, Japan). The aldehyde-modified PEG2000 (DF-PEG2000) was purchased from Yaribo Co. Ltd. (Shanghai, China). The anticancer drug doxorubicin hydrochloride (DOX) was supplied by Shanghai Jinhe Bio-Technology Co. Ltd. (Shanghai, China). Dulbecco's modified Eagle's medium (DMEM), Roswell Park Memorial Institute (RPMI) 1640 medium, fetal bovine serum (FBS), penicillin–streptomycin (PS), and trypsin were bought from Gibco Life Technologies (Beijing, China). 4T1, MCF-7, and L929 cells were obtained from the American type culture collection (ATCC). Female BALB/c mice were obtained from Weitong River Laboratory Animal Technology Co., Ltd. (Beijing, China).

Methods. *Preparation and Characterization of HTS-PEG Hydrogels.* The hydrogel was prepared according to our previous publications.[29,43] Briefly, 4% (w/w) glycol chitosan solution and 3% (w/w) DF-PEG_{2000} solution were prepared by dissolving glycol chitosan or DF-PEG_{2000} in an 8.0−15.0% (w/w) sodium chloride aqueous solution. As a typical hydrogel preparation, equal volumes of glycol chitosan and DF-PEG_{2000} solution were mixed uniformly to get the gelation within ∼60 s. The control hydrogel was prepared without the saline solution. Prior to all animal experiments and cell experiments, the as-prepared hydrogel was sterilized with an ultraviolet lamp for 24 h.

Fourier transform infrared spectra (FT-IR) were obtained by model VERTEX80 Fourier transform infrared spectrometer at room temperature (Bruker, Germany). The morphology of the HTS-PEG hydrogel was characterized by FESEM. Equilibrium swelling ratio and degradation of the hydrogel were measured gravimetrically. Rheology analyses were carried out using a TA-AR2000 rheometer (TA instruments) with a parallel plate geometry at 37 °C. The morphology of the hydrogels was characterized by FESEM. The capacitance of the saline solution was measured by a precision impedance analyzer (4294A, Agilent).

Inductive Heating Properties of HTS Solutions and HTS-PEG Hydrogel under AMF Exposure. The inductive heating properties of the NaCl (HTS) and other kinds of inorganic salt solutions were evaluated using 1 mL of salt solutions with different concentrations contained in a 5 mL EP centrifugal tube. The PE tubes were placed in the middle of a copper induction coil and exposed under an AC magnetic field at a frequency (f) of 495 kHz and field intensities (H) of 150, 220, and 285 Oe. The change in temperature was continuously logged by fiber optic probes inserted within PE tubes, and the heating curves with time were plotted. In addition, the HTS-PEG hydrogels were subjected to three rounds of repeated exposure using AMF on/off cycling (495 kHz, 220 Oe) in ∼15 min intervals to investigate their magnetic heating reproducibility.

Dielectric Constant Measurement of Different Saline Solutions. The dielectric constant (ε') of different kinds of ion solutions was tested on a precision impedance analyzer with a man-made box. The frequency dependence of the dielectric constant can be calculated by measuring the capacitance using the below formula

$$\varepsilon' = \frac{C \times d}{A}$$

where C is the capacitance, A is the area of the two plates, and d is the separated distance of the two plates.

Ion Confinement Effect of Hydrogel Formulation. The ion confinement efficiency of the HTS-PEG hydrogel was evaluated by a self-designed temperature measurement system. Agar phantom (8 mL, 4% (w/w), agar powder, 0.6% (w/w) NaCl, and 95.4% (w/w) water) was added into a 15 mL centrifuge tube, and a 4 mL 15% HTS-PEG hydrogel was transferred into the centrifuge tube on top of the agar phantom. Three optical fibers were fixed within the system, with one probe put in the center of the HTS-PEG hydrogel ($T1$) and the other two below it at distances of 6.5 and 10.5 mm ($T2$ and $T3$, as illustrated in Scheme 2). At different time intervals of 0, 12, 24, and 48 h, the centrifuge tube containing the phantom and hydrogel system was exposed under AMF for 6 min. Temperatures of the three positions, namely, $T1$, $T2$, and $T3$, were continuously measured and compared.

Rheology Analyses of HTS-PEG Hydrogels. As a typical operation, a 0.2 mL GC HTS solution was spread on a parallel plate. Then, a 0.2 mL DF-PEG_{2000} HTS solution was added dropwise onto the surface of the GC solution evenly, and the samples were applied to the rheometer. The storage moduli G' and loss moduli G'' were collected to monitor the gelation process in an oscillatory mode. The value of the critical strain region (gel transfer to sol) was detected using the strain amplitude sweep method. The change in modulus values versus

DOI: 10.1021/acsami.9b02013
ACS Appl. Mater. Interfaces XXXX, XXX, XXX−XXX

Scheme 2. Design for Temperature Measurement System Based on Agar Phantom/HTS-PEG Hydrogel

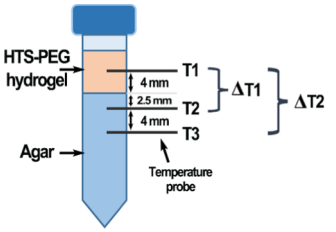

frequency or strain was analyzed by the samples prepared using the above method and incubated for 20 min before data collection.

In Vitro Hydrolytic Degradation and pH-Dependent Drug Release with or without Exposure under AMF. The in vitro hydrolytic degradation of the hydrogel was performed under simulated physiological environment. Briefly, each lyophilized hydrogel was divided into two groups. Group I was immersed in 10 mL of PBS (pH = 7.4) and group II was immersed in 10 mL of PBS (pH = 6.5). Weight loss was performed as a function of incubation time at 37 °C. At determined time points, the samples were lyophilized, and the change in weight was measured. The weight remaining rate (%) at each time interval was determined using the equation

$$\text{weight remaining rate} = \frac{W_0 - W_t}{W_0} \times 100\% \quad (2)$$

where W_0 is the beginning weight of each sample and W_t is the dry weight of the degraded hydrogels at different time intervals. All results were estimated from the data of three individual experiments.

Drug release for extended time periods was studied at different pH values with or without AMF exposure. Samples of 1 mL hydrogels with 2.0 mg mL^{-1} DOX were sealed into a dialysis bag (cutoff molecular weight of 3000 Da). These dialysis bags were kept in the plastic centrifuge tubes and, respectively, immersed in 20 mL of PBS (pH = 7.4 and 6.5) in 37 °C water bath with occasional stirring. Release medium (1 mL) was extracted and replaced with fresh PBS, periodically. The vials were shaken in darkness at 37 °C. To investigate the role of AMF exposure on drug release, parallel drug release experiments were conducted on two samples of approximately the same weight, with one subjected to the AMF (f = 495 kHz, H = 220 Oe) for 10 min at different time intervals and another one as a control. Determination of DOX release and the cumulative DOX release were calculated with a spectrophotometer measurement at an absorbance value of 480 nm. Results were estimated from the data of three individual experiments.

In Vivo Antitumor Efficacy of the DOX-Loaded Hydrogel. All animal studies were conducted in accordance with the experimental protocols involving animal study approved by the Institutional Animal Care and Use Committee of Tsinghua University. All of the animals were kept at a pathogen-free condition, maintained under artificial day−night cycles (12 h light−dark cycles; 23 °C room temperature, 30−60% environment humidity), and received food and water ad libitum.

To establish the tumor model, mice were subcutaneously injected in the left back with 5×10^6 MCF-7 or 4T1 cells. The mice were randomly assigned to five groups (n = 4 for each group). When the volumes of tumor reached around ∼0.2 cm^3, the ∼2/3 of the tumor were removed by surgery with 1/3 left to simulate the residual tumor bed for postoperative recurrence. Mice were treated with saline (group 1), DOX-hydrogel (group 2), HTS-PEG hydrogel (group 3), HTS-PEG hydrogel + AMF (group 4), and DOX-HTS-PEG hydrogel + AMF (group 5). After 24 h of implantation, the mice in groups 4 and 5 were anesthetized and placed in an AMF (495 kHz, 220 Oe) for hyperthermia treatment about 12 min. The temperature distribution was recorded by fiber optic probes inserted within the tumor and rectal. Mice were monitored in the following weeks for survival and tumor profiling. Animal weight and tumor volume were measured and calculated once every 2 or 3 days for 27 days. The animals were then sacrificed and the tumor volume (V) was calculated using the following equation

$$V = \frac{L \times W^2}{2} \quad (3)$$

where the length (L) is the longest diameter and the width (W) is the shortest diameter perpendicular to the length. The tumor volumes are normalized against the original volumes (V_0) for monitoring the tumor growth process. All mice were monitored every other day for body weight and tumor size. At day 27, mice were cervically dislocated under an anesthetic status, and major organs (heart, liver, spleen, lung, and kidney) and tumors were removed, immersed in 4% buffered paraformaldehyde for 48 h, and embedded in paraffin. The paraffin-embedded tissue samples of the implanted tumor were sliced and stained with hematoxylin and eosin (H&E) for histopathological changes evaluated by microscopy.

Statistical Analysis. All of the experimental data were presented as the mean ± standard deviation (SD) values. Statistical analysis was conducted using one-way ANOVA followed by post hoc t test with the least significant difference method using the SPSS (IBM7 SPSS version 23) to evaluate differences between two groups. Values of P, which were less than 0.05, were considered statistically significant.

■ ASSOCIATED CONTENT

Supporting Information

The Supporting Information is available free of charge on the ACS Publications website at DOI: 10.1021/acsami.9b02013.

The thermal images of HTS with different saline concentrations (Figure S1); the dielectric constant of HTS (Figure S2); the FT-IR spectra (Figure S3); in vitro drug cumulative release profiles (Figure S4); and changes in relative body weight of MCF-7 and 4T1 tumor-bearing mice (Figure S5) (PDF)

■ AUTHOR INFORMATION

Corresponding Authors

*E-mail: weiyen@tsinghua.edu.cn (Y.W.).
*E-mail: fanhm@nwu.edu.cn (H.M.F.).
*E-mail: lyzhao@mail.tsinghua.edu.cn (L.Z.).

ORCID

Wensheng Xie: 0000-0002-1291-3427
Xing Wang: 0000-0002-9990-1479
Lei Tao: 0000-0002-1735-6586
Lingyun Zhao: 0000-0001-8799-7496

Notes

The authors declare no competing financial interest.

■ ACKNOWLEDGMENTS

The authors wish to acknowledge the financial support provided by the National Natural Science Foundation of China (Grant Nos. 81671829, 81771981, 81571809, and 21376192) and the Postdoctoral Science Foundation of China (2018M641010).

■ REFERENCES

(1) Beik, J.; Abed, Z.; Ghoreishi, F. S.; Hosseini-Nami, S.; Mehrzadi, S.; Shakeri-Zadeh, A.; Kamrava, S. K. Nanotechnology in Hyperthermia Cancer Therapy: From Fundamental Principles to Advanced Applications. *J. Controlled Release* **2016**, *235*, 205−221.

(2) Fan, W.; Yung, B.; Huang, P.; Chen, X. Nanotechnology for Multimodal Synergistic Cancer Therapy. *Chem. Rev.* **2017**, *117*, 13566−13638.

DOI: 10.1021/acsami.9b02013
ACS Appl. Mater. Interfaces XXXX, XXX, XXX−XXX

(3) Gazeau, F.; Levy, M.; Wilhelm, C. Optimizing Magnetic Nanoparticles Design for Nanothermotherapy. *Nanomedicine* **2008**, *3*, 831−844.
(4) Cazares-Cortes, E.; Cabana, S.; Boitard, C.; Nehlig, E.; Griffete, N.; Fresnais, J.; Wilhelm, C.; Abou-Hassan, A.; Menager, C. Recent Insights in Magnetic Hyperthermia: From the "Hot-spot" Effect for Local Delivery to Combined Magneto-photo-thermia using Magneto-plasmonic Hybrids. *Adv. Drug Delivery Rev.* **2018**, DOI: 10.1016/j.addr.2018.10.016.
(5) Lee, J. H.; Jang, J. T.; Choi, J. S.; Moon, S. H.; Noh, S. H.; Kim, J. W.; Kim, J. G.; Kim, I. S.; Park, K. I.; Cheon, J. Exchange-coupled Magnetic Nanoparticles for Efficient Heat Induction. *Nat. Nanotechnol.* **2011**, *6*, 418−422.
(6) Thiesen, B.; Jordan, A. Clinical Applications of Magnetic Nanoparticles for Hyperthermia. *Int. J. Hyperthermia* **2008**, *24*, 467−474.
(7) Singh, D.; McMillan, J. M.; Kabanov, A. V.; Sokolsky-Papkov, M.; Gendelman, H. E. Bench-to-Bedside Translation of Magnetic Nanoparticles. *Nanomedicine* **2014**, *9*, 501−516.
(8) Chiu-Lam, A.; Rinaldi, C. Nanoscale Thermal Phenomena in the Vicinity of Magnetic Nanoparticles in Alternating Magnetic Fields. *Adv. Funct. Mater.* **2016**, *26*, 3933−3941.
(9) Moroz, P.; Jones, S. K.; Gray, B. N. Magnetically Mediated Hyperthermia: Current Status and Future Directions. *Int. J. Hyperthermia* **2002**, *18*, 267−284.
(10) Guisasola, E.; Asin, L.; Beola, L.; de la Fuente, J. M.; Baeza, A.; Vallet-Regi, M. Beyond Traditional Hyperthermia: In Vivo Cancer Treatment with Magnetic-Responsive Mesoporous Silica Nanocarriers. *ACS Appl. Mater. Interfaces* **2018**, *10*, 12518−12525.
(11) Tong, S.; Quinto, C. A.; Zhang, L.; Mohindra, P.; Bao, G. Size-Dependent Heating of Magnetic Iron Oxide Nanoparticles. *ACS Nano* **2017**, *11*, 6808−6816.
(12) Mai, B. T.; Balakrishnan, P. B.; Barthel, M. J.; Piccardi, F.; Niculaes, D.; Marinaro, F.; Fernandes, S.; Curcio, A.; Kakwere, H.; Autret, G.; Cingolani, R.; Gazeau, F.; Pellegrino, T. Thermo-Responsive Iron Oxide Nanocubes for an Effective Clinical Translation of Magnetic Hyperthermia and Heat-Mediated Chemotherapy. *ACS Appl. Mater. Interfaces* **2019**, DOI: 10.1021/acsami.8b16226.
(13) Noh, S. H.; Na, W.; Jang, J. T.; Lee, J. H.; Lee, E. J.; Moon, S. H.; Lim, Y.; Shin, J. S.; Cheon, J. Nanoscale Magnetism Control via Surface and Exchange Anisotropy for Optimized Ferrimagnetic Hysteresis. *Nano Lett.* **2012**, *12*, 3716−3721.
(14) Liu, X. L.; Yang, Y.; Ng, C. T.; Zhao, L. Y.; Zhang, Y.; Bay, B. H.; Fan, H. M.; Ding, J. Magnetic Vortex Nanorings: a New Class of Hyperthermia Agent for Highly Efficient in vivo Regression of Tumors. *Adv. Mater.* **2015**, *27*, 1939−1944.
(15) Bourquin, J.; Milosevic, A.; Hauser, D.; Lehner, R.; Blank, F.; Petri-Fink, A.; Rothen-Rutishauser, B. Biodistribution, Clearance, and Long-Term Fate of Clinically Relevant Nanomaterials. *Adv. Mater.* **2018**, *30*, No. e1704307.
(16) Hartshorn, C. M.; Bradbury, M. S.; Lanza, G. M.; Nel, A. E.; Rao, J.; Wang, A. Z.; Wiesner, U. B.; Yang, L.; Grodzinski, P. Nanotechnology Strategies To Advance Outcomes in Clinical Cancer Care. *ACS Nano* **2018**, *12*, 24−43.
(17) Naha, P. C.; Liu, Y.; Hwang, G.; Huang, Y.; Gubara, S.; Jonnakuti, V.; Simon-Soro, A.; Kim, D.; Gao, L.; Koo, H.; Cormode, D. P. Dextran Coated Iron Oxide Nanoparticles as Biomimetic Catalysts for Localized and pH-Activated Biofilm Disruption. *ACS Nano* **2019**, DOI: 10.1021/acsnano.8b08702.
(18) Lemal, P.; Geers, C.; Rothen-Rutishauser, B.; Lattuadaa, M.; Petri-Fink, A. Measuring the Heating Power of Magnetic Nanoparticles: an Overview of Currently Used Methods. *Mater. Today* **2017**, *4*, S107−S117.
(19) Bhardwaj, A.; Ulatowski, J. A. Hypertonic Saline Solutions in Brain Injury. *Curr. Opin. Crit. Care* **2004**, *10*, 126−131.
(20) Wu, S.; Baker, C.; Lang, M. E.; Schrager, S. M.; Liley, F. F.; Papa, C.; Mira, V.; Balkian, A.; Mason, W. H. Nebulized Hypertonic Saline for Bronchiolitis: a Randomized Clinical Trial. *JAMA Psychiatry* **2014**, *168*, 657−663.
(21) Kamel, H.; Navi, B. B.; Nakagawa, K.; Hemphill, J. C., 3rd; Ko, N. U. Hypertonic Saline versus Mannitol for the Treatment of Elevated Intracranial Pressure: a Meta-Analysis of Randomized Clinical Trials. *Crit. Care Med.* **2011**, *39*, 554−559.
(22) Wade, C. E.; Kramer, G. C.; Grady, J. J.; Fabian, T. C.; You, R. N. Efficacy of Hypertonic 7.5% Saline and 6% Dextran-70 in Treating Trauma: A Meta-Analysis of Controlled Clinical Studies. *Surgery* **1997**, *122*, 609−616.
(23) Qi, Y.; Min, H.; Mujeeb, A.; Zhang, Y.; Han, X.; Zhao, X.; Anderson, G. J.; Zhao, Y.; Nie, G. Injectable Hexapeptide Hydrogel for Localized Chemotherapy Prevents Breast Cancer Recurrence. *ACS Appl. Mater. Interfaces* **2018**, *10*, 6972−6981.
(24) Menéndez, J. A.; Arenillas, A.; Fidalgo, B.; Fernández, Y.; Zubizarreta, L.; Calvo, E. G.; Bermúdez, J. M. Microwave Heating Processes Involving Carbon Materials. *Fuel Process. Technol.* **2010**, *91*, 1−8.
(25) Zlotorzynski, A. The Application of Microwave Radiation to Analytical and Environmental Chemistry. *Crit. Rev. Anal. Chem.* **1995**, *25*, 43−76.
(26) George, S. C.; Thomas, S. Transport Phenomena Through Polymeric Systems. *Prog. Polym. Sci.* **2001**, *26*, 985−1017.
(27) Wu, Y.; Joseph, S.; Aluru, N. R. Effect of Cross-Linking on the Diffusion of Water, Ions, and Small Molecules in Hydrogels. *J. Phys. Chem. B* **2009**, *113*, 3512−3520.
(28) Hoffman, A. S. Hydrogels for Biomedical Applications. *Adv. Drug Delivery Rev.* **2012**, *64*, 18−23.
(29) Xie, W.; Gao, Q.; Guo, Z.; Wang, D.; Gao, F.; Wang, X.; Wei, Y.; Zhao, L. Injectable and Self-Healing Thermosensitive Magnetic Hydrogel for Asynchronous Control Release of Doxorubicin and Docetaxel to Treat Triple-Negative Breast Cancer. *ACS Appl. Mater. Interfaces* **2017**, *9*, 33660−33673.
(30) Li, J.; Mooney, D. J. Designing Hydrogels for Controlled Drug Delivery. *Nat. Rev. Mater.* **2016**, *1*, No. 16071.
(31) Li, Y.; Liu, C.; Tan, Y.; Xu, K.; Lu, C.; Wang, P. In situ Hydrogel Constructed by Starch-based Nanoparticles via a Schiff base Reaction. *Carbohydr. Polym.* **2014**, *110*, 87−94.
(32) Zhang, Y.; Tao, L.; Li, S.; Wei, Y. Synthesis of Multiresponsive and Dynamic Chitosan-based Hydrogels for Controlled Release of Bioactive Molecules. *Biomacromolecules* **2011**, *12*, 2894−2901.
(33) Zhang, Z. Q.; Song, S. Thermosensitive/Superparamagnetic Iron Oxide Nanoparticle-loaded Nanocapsule Hydrogels for Multiple Cancer Hyperthermia. *Biomaterials* **2016**, *106*, 13−23.
(34) Li, Y.; Rodrigues, J.; Tomas, H. Injectable and Biodegradable Hydrogels: Gelation, Biodegradation and Biomedical Applications. *Chem. Soc. Rev.* **2012**, *41*, 2193−2221.
(35) Razmjou, A.; Liu, Q.; Simon, G. P.; Wang, H. Bifunctional Polymer Hydrogel Layers as Forward Osmosis Draw Agents for Continuous Production of Fresh Water Using Solar Energy. *Environ. Sci. Technol.* **2013**, *47*, 13160−13166.
(36) Ricka, J.; Tanaka, T. Swelling of Ionic Gels: Quantitative Performance of the Donnan Theory. *Macromolecules* **1984**, *17*, 2916−2921.
(37) Li, D.; Zhang, X.; Yao, J.; Zeng, Y.; Simon, G. P.; Wang, H. Composite Polymer Hydrogels as Draw Agents in Forward Osmosis and Solar Dewatering. *Soft Matter* **2011**, *7*, 10048−10056.
(38) Xin, Y.; Yuan, J. Schiff's Base as a Stimuli-responsive Linker in Polymer Chemistry. *Polym. Chem.* **2012**, *3*, 3045−3055.
(39) Brulé, S.; Levy, M.; Wilhelm, C.; Letourneur, D.; Gazeau, F.; Menager, C.; Le Visage, C. Doxorubicin Release Triggered by Alginate Embedded Magnetic Nanoheaters: a Combined Therapy. *Adv. Mater.* **2011**, *23*, 787−790.
(40) Lao, L.; Ramanujan, R. Magnetic and Hydrogel Composites Materials for Hyperthermia Applications. *J. Mater. Sci.: Mater. Med.* **2004**, *15*, 1061−1064.
(41) Brandl, F.; Kastner, F.; Gschwind, R. M.; Blunk, T.; Tessmar, J.; Gopferich, A. Hydrogel-based Drug Delivery Systems: Comparison of Drug Diffusivity and Release Kinetics. *J. Controlled Release* **2010**, *142*, 221−228.

DOI: 10.1021/acsami.9b02013
ACS Appl. Mater. Interfaces XXXX, XXX, XXX−XXX

(42) Merino, S.; Martí, C.; Kostarelos, K.; Prato, M.; zquez, E. V. Nanocomposite Hydrogels: 3D Polymer Nanoparticle Synergies for On-Demand Drug Delivery. *ACS Nano* **2015**, *9*, 4686−4697.
(43) Li, Y.; Wang, X.; Fu, Y. N.; Wei, Y.; Zhao, L.; Tao, L. Self-Adapting Hydrogel to Improve the Therapeutic Effect in Wound-Healing. *ACS Appl. Mater. Interfaces* **2018**, *10*, 26046−26055.

DOI: 10.1021/acsami.9b02013
ACS Appl. Mater. Interfaces XXXX, XXX, XXX−XXX